

Multi-Material Beam Hardening Correction(MMBHC) in Computed Tomography

Qiao Yang, Nicole Maass, Mengqiu Tian, Matthias Elter, Ingo Schasiepen, Andreas Maier, and Joachim Hornegger

Abstract—In computed tomography (CT), the nonlinear attenuation characteristics of polychromatic X-rays cause beam hardening artifacts in the reconstructed images. State-of-the-art methods to correct the beam hardening effect are mostly single material pre-corrections (e.g. water-precorrection), which are far less efficient when more than one material is present in the field of measurement. The use of those techniques is limited by specific restrictions to the objects, computational loads, and inaccurate segmentations. In this paper, we present a practical multi-material beam hardening correction(MMBHC) approach that employs material decomposition technique maintaining CT values from dual-energy CT. This separates single energy CT images into spatial density images and images containing material information. The segmentation maintains the original X-ray attenuation coefficients, such that the original CT attenuation image can be exactly recovered. Therefore, segmentation errors, which result in invalid material properties to the voxel, only have minor effects on the beam hardening correction and do not cause an atypical image impression or introduce additional artifacts. A multi-material beam hardening correction procedure is formulated to iteratively correct the artifacts but shows satisfactory image quality after the first iteration. Based on experiments with simulated CT data, it is shown that the proposed method can efficiently reduce beam hardening artifacts. In addition to the performance benefits, our approach can be flexibly applied to imaging geometries and achieve efficient, fully 3D reconstructions.

Index Terms—CT reconstruction, beam hardening, artifact reduction, segmentation, spatial resolution, image quality

I. INTRODUCTION

In computed tomography (CT), standard reconstruction techniques are generally based on the assumption that the X-ray beams are monochromatic and the measured projection images contain line integrals through the objects. However, in practice, the X-rays are polychromatic and lower energy photons are more easily absorbed than the higher energy photons, resulting in nonlinear characteristics of the X-rays, the so-called beam hardening phenomenon. The polychromatic characteristic of X-rays leads to the attenuation of a homogeneous object not being proportional to the thickness of the object along the ray. Consequently, severe artifacts such as cupping and streak artifacts appear in the reconstruction, which compromise the reconstruction quality and diagnostic

Q. Yang, Dr. Andreas Maier and Prof. Dr. J. Hornegger are with the Pattern Recognition Lab, Department of Computer Science, Friedrich-Alexander-University Erlangen-Nuremberg, Martenstrasse 3, Erlangen, Germany and the Erlangen Graduate School Heterogeneous Imaging Systems. Dr. Andreas Maier and Prof. Dr. J. Hornegger are with the Erlangen Graduate School in Advanced Optical Technologies (SAOT). Q. Yang, Dr. N. Maass, M. Tian, Dr. M. Elter and I. Schasiepen are with the Siemens AG, Healthcare Sector, Erlangen, Germany. This work was partly supported by the Research Training Group 1773 "Heterogeneous Image Systems", funded by the German Research Foundation (DFG).

Corresponding author: qiao.yang@cs.fau.de.

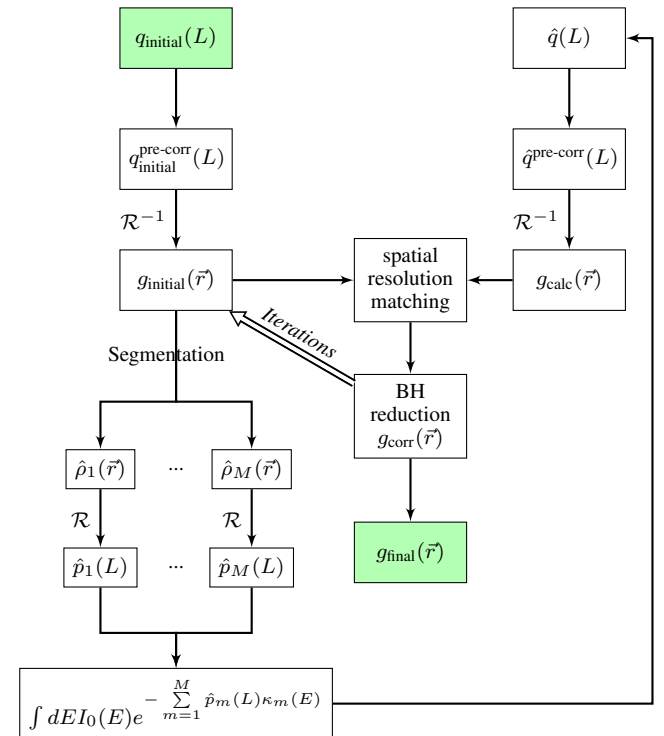


Fig. 1: Flowchart of our proposed algorithm

accuracy. Therefore, an effective beam hardening correction approach is important in both medical and industrial CT applications to improve image quality.

To mitigate beam hardening, common methods are hardware-based approaches to reduce the polychromaticity of the incident X-rays. State-of-the-art beam hardening correction (BHC) algorithms used in clinical CT are mainly based on single material (e.g. water) calibration and can efficiently correct objects consisting of materials that are spectrally alike [1]. In dual energy CT, the aim is oftentimes to reconstruct images of material densities and as a side-effect, the beam hardening artifacts can be exactly corrected [2]–[5].

In this work, we focus on the single energy CT of objects that consist of multiple materials (with different spectral properties). Prior research on this topic requires a segmentation of the attenuation image from a single energy CT scan into different materials [6]–[14]. A major limitation of these techniques is the computational complexity. Moreover, require previous knowledge, the objects' characteristics such as number of materials, material's inhomogeneity and the shape of different materials also render those techniques unsuitable for practical usage. The high computational load of these methods is often

caused by missegmentation of materials in early iterations, which slows down convergence and may result in atypical image impression and additional artifacts.

We present an application of the dual-energy reconstruction technique presented in reference [5] with a sophisticated segmentation method which makes it applicable to single energy CT. Both methods calculate polychromatic raw data from material density images of base materials. While the calculation of base material density images is the aim of dual energy CT, we use maintained CT attenuation values for segmentation in single energy CT to generate material density images. Thereby, the CT attenuation value conservation leads to a situation where the consequences of missegmentation in the beam hardening correction are minor. We do not make any assumptions on the scanned object, but we assume to know the major materials' spectral properties, of which the object is composed. This knowledge may be obtained from a single calibration scan [4].

Section II outlines the theoretical aspects of the proposed algorithm. The method has been evaluated for simulated X-ray CT data, which is presented in section IV. Finally, we discuss relevant issues to conclude the paper in section V.

II. METHODS

Assume a dataset consists of M materials with attenuation coefficients $\mu_m(E)$, $m = 1, \dots, M$, which depend on the X-ray photon energy E . Specifying a reference density of each material, ρ_m , the mass attenuation coefficient for material m is $\kappa_m(E) = \mu_m(E)/\rho_m$. Denote \vec{r} as spatial location on reconstruction grid. Knowing the spatial density distributions $\rho_m(\vec{r})$ and effective energy E_0 , the monochromatic CT attenuation image can be calculated:

$$f(\vec{r}) = \sum_{m=1}^M \rho_m(\vec{r}) \kappa_m(E_0). \quad (1)$$

$p_m(L) = \int_L dl \rho(\vec{r})$ is the line integral over projection ray L through a material density image $\rho(\vec{r})$. When a monochromatic X-ray beam traverses a homogeneous object, according to Lambert-Beer's law, the total attenuation coefficient is linearly related to the thickness of the object along the ray. The monochromatic intensity for a given E_0 can be expressed as

$$I_{\text{mono}}(L) = I_0(E_0) \cdot e^{-\sum_{m=1}^M p_m(L) \kappa_m(E_0)}. \quad (2)$$

However, in real CT, the emitted X-ray photons have varying energies $E \in [0, E_{max}]$. Therefore, the measured intensity of a polychromatic beam can be written as the sum of the monochromatic contributions for each energy E :

$$I_{\text{poly}}(L) = \int dE I_0(E) e^{-\sum_{m=1}^M p_m(L) \kappa_m(E)}, \quad (3)$$

where $I_0(E)$ is referred as normalized source-detector energy spectrum ($\int dE I_0(E) = 1$). The measured initial polychromatic attenuation $q_{\text{initial}}(L)$ along a ray path L is defined by

$$q_{\text{initial}}(L) = -\ln I_{\text{poly}}(L). \quad (4)$$

A. Single-material precorrection

Generally, when datasets consist of only one material, a precorrection can be carried out to reduce cupping artifacts caused by beam hardening. In clinical CT, water precorrection is widely used to reduce cupping artifacts. In industrial CT we usually precorrect for the most dominant material (i.e. the material which covers the most volume). The single material precorrection linearizes the projections at the first place in order to deliver improved and quantitative reconstruction for a better initial segmentation. In any case, the single material precorrection is a nonlinear preprocessing step of the initial rawdata:

$$q_{\text{initial}}^{\text{precorr}}(L) = q_{\text{initial}}^{\text{precorr}}(q_{\text{initial}}(L)). \quad (5)$$

B. Multi-material correction approach

A flowchart of the proposed algorithm is illustrated in Fig. 1. From the precorrected rawdata, we perform a preliminary filtered backprojection

$$g_{\text{initial}}(\vec{r}) = \mathcal{R}^{-1}\{q_{\text{initial}}^{\text{precorr}}(L)\}, \quad (6)$$

where \mathcal{R}^{-1} denotes a filtered backprojection (FBP) reconstruction. The initial reconstruction is then segmented into M materials. We thereby require to know the number M of significant materials and the mass attenuation coefficient of these materials. The spectral properties can either be calibrated [4] or obtained as tabulated data from reference [15]. As quantitative CT values in the image are unreliable due to beam hardening, we use automatic centroids selection for k-means clustering [16], [17]. After segmenting $g_{\text{initial}}(\vec{r})$ into M masks $w_m(\vec{r})$, we maintain the original CT value by storing density volumes

$$\hat{\rho}_m(\vec{r}) = \frac{w_m(\vec{r}) \cdot g_{\text{initial}}(\vec{r})}{\kappa_m(E_0)}, \quad (7)$$

rather than the mask volumes $w_m(\vec{r})$. From the selected centroids at k-means clustering, effective energy E_0 can be obtained by choosing corresponding monochromatic energy at the centroid attenuation coefficients for each material. From the segmentation result, the CT attenuation image $g_{\text{initial}}(\vec{r})$ could be calculated according to Eq. (1). For each material, line integrals

$$\hat{p}_m(L) = \mathcal{R}\{\hat{\rho}_m(\vec{r})\} = \int_L dl \hat{\rho}_m(\vec{r}) \quad (8)$$

are calculated, where \mathcal{R} denotes the calculation of line integrals through the volume along the originally measured lines L (forward projection). The line integrals are combined to a polychromatic rawdata set

$$\hat{q}(L) = -\ln \int dE I_0(E) e^{-\sum_{m=1}^M \hat{p}_m(L) \kappa_m(E)}, \quad (9)$$

which incorporates the spectral properties of each material $\kappa_m(E)$, as mentioned above. The polychromatic rawdata are then reconstructed again (including the single material precorrection) to obtain a recalculated image

$$g_{\text{calc}}(\vec{r}) = \mathcal{R}^{-1}\{\hat{q}^{\text{precorr}}(L)\}. \quad (10)$$

During segmentation and forward projection steps, errors which arise from beam hardening are additionally introduced.

The difference between the initially reconstructed volume and the recalculated volume can be used to estimate the beam hardening error:

$$g_{\text{BH}}(\vec{r}) = g_{\text{calc}}(\vec{r}) - g_{\text{initial}}(\vec{r}). \quad (11)$$

It has to be noted that spatial resolution mismatch occurs between $g_{\text{initial}}(\vec{r})$ and $g_{\text{calc}}(\vec{r})$. Therefore, a spatial resolution matching technique should be applied before the subtraction to maintain the spatial resolution of the final image. In general, resolution can be modulated by using boosting or smoothing kernels. In this paper, an optimized Gaussian smoothing kernel is applied to $g_{\text{initial}}(\vec{r})$ before the subtraction, such that

$$\hat{g}_{\text{BH}}(\vec{r}) = g_{\text{calc}}(\vec{r}) - \text{Gauss}(0, \sigma) * g_{\text{initial}}(\vec{r}), \quad (12)$$

with $\arg \min_{\sigma} \|\hat{g}_{\text{BH}}(\vec{r})\|_2$. We finally use the spatially resolution-matched beam hardening image $\hat{g}_{\text{BH}}(\vec{r})$ to subtract the beam hardening from the initial reconstruction.

$$g_{\text{corrected}}(\vec{r}) = g_{\text{initial}}(\vec{r}) - \hat{g}_{\text{BH}}(\vec{r}). \quad (13)$$

As the corrected image could be used to obtain a better segmentation in the first place, the method can be repeated iteratively. Using the superset $i \geq 0$ to denote the iteration number and initializing with $g_{\text{corrected}}^0(\vec{r}) = g_{\text{initial}}(\vec{r})$, we can formulate a fixed-point equation

$$g_{\text{corrected}}^{i+1}(\vec{r}) = g_{\text{initial}}(\vec{r}) - \hat{g}_{\text{BH}}(g_{\text{corrected}}^i(\vec{r})). \quad (14)$$

III. EXPERIMENTS

To evaluate the proposed algorithm, polychromatic cone-beam CT simulations were carried out using a FORBILD hip prosthesis phantom [18]. The dataset consists of soft tissue, bone, and the prosthesis (Ti). The projection data were obtained by using CT simulation software DRASIM (Siemens AG, Forchheim, Germany), and circular 3D raw data were reconstructed using a standard FDK reconstruction algorithm [19]. At a tube voltage of 100 kV we simulated 450 angular samples on a full circle, with a detector of 512×512 pixels, 0.5mm in pixel size. All projection images are reconstructed on a $512 \times 512 \times 512$ grid with a voxel size of 0.4mm.

For further examination of the algorithm, a real multi-material dataset containing four cylinders of different materials was evaluated. A 120 kV tube voltage was applied. Detector pixels are 1024×1024 with size of 0.4mm. All projection images are reconstructed on a $400 \times 400 \times 600$ grid with a voxel size of 0.5mm.

IV. RESULTS AND DISCUSSION

A. Beam hardening reduction

Fig. 2 and Fig. 4 illustrate the results from reconstructions and horizontal line profiles for simulated and real datasets, respectively. In comparison with original reconstructions (left), the recalculated polychromatic (middle) images show enhanced beam hardening artifacts. This illustrates our assumption in Eq. (12). The right figures show the final result, where beam hardening artifacts are hardly noticeable and the spatial resolution is maintained.

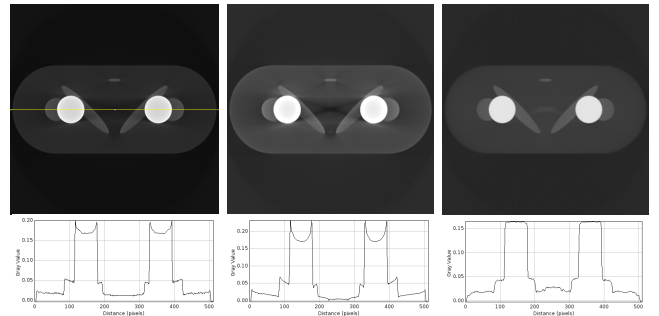


Fig. 2: Reconstruction results from hip prosthesis phantom with corresponding horizontal line profiles (yellow line). From left to right: original reconstruction, recalculated reconstruction, result after first iteration. The line profiles and images show attenuation coefficients (Level 0.10; window 0.22.)

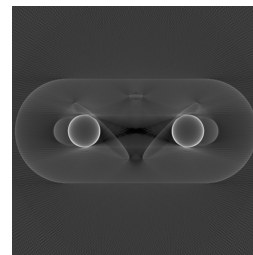


Fig. 3: The beam hardening image $\hat{g}_{\text{BH}}(\vec{r})$ according to Eq. 12.

B. Spatial resolution matching

In Fig. 3 the beam hardening image $\hat{g}_{\text{BH}}(\vec{r})$ according to equation 12 is presented. The enhancement of object borders is visible from this image remains after spatial resolution matching and is caused by beam hardening.

Running a forward projection with subsequent reconstruction reduces the spatial resolution of an image. Calculating the difference between original and recalculated images would correspond to a high-pass filtering of the original image. As the initial image is linearly combined with the difference image, we need measurements to maintain the spatial resolution, especially when more than one iteration is applied.

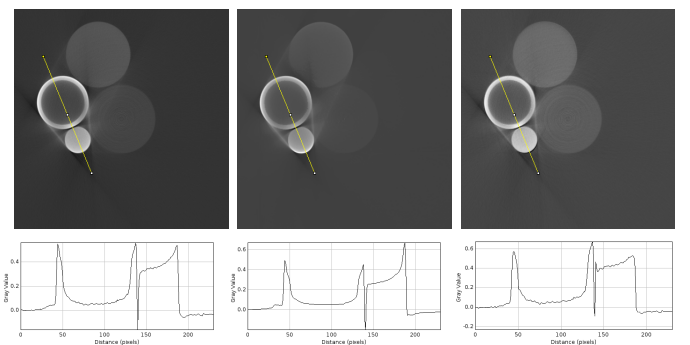


Fig. 4: Reconstruction results from 4-cylinder real dataset with corresponding horizontal line profiles (yellow line). From left to right: original reconstruction, recalculated reconstruction, result after first iteration. The line profiles and images show attenuation coefficients.

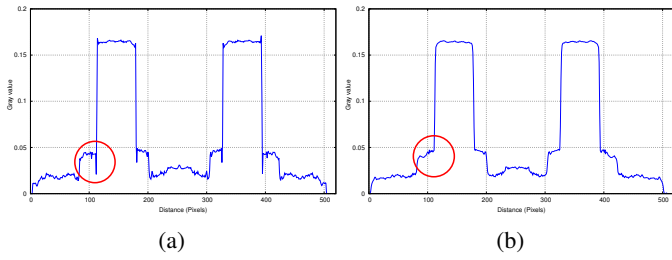


Fig. 5: Horizontal line profile plots from corrected reconstructions with (a) and without (b) spatial resolution matching.

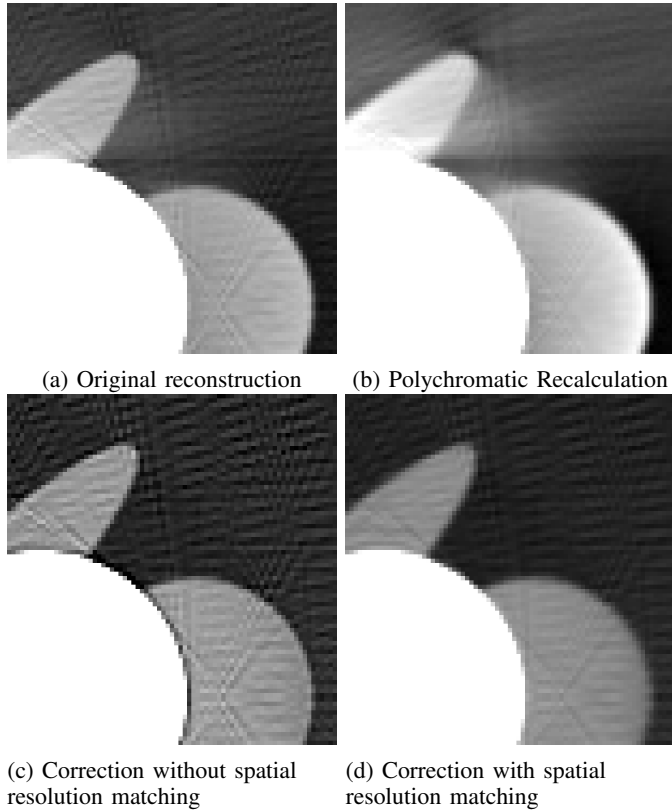


Fig. 6: Examination of spatial resolution matching using a zoom-in on the hip prosthesis phantom (Grayscale: level 0.04; window 0.06).

Fig. 5 presents the line profiles from reconstructions with (Fig. 5a) and without (Fig. 5b) the spatial resolution matching. It can be seen that calculation without consideration of resolution matching yields errors at object edges (red circle) and increases the level of aliasing.

A closer evaluation of spatial resolution influences on reconstructions of the hip prosthesis phantom are illustrated in Fig. 6. The polychromatic recalculation (Fig. 6b) has a lower resolution than the original reconstruction (Fig. 6a). Additionally, the enhanced cupping and streak artifacts can be noticed. Running the proposed method without spatial resolution matching, the object edges appear over-enhanced and the aliasing is increased as shown in Fig. 6c. However, if spatial resolution matching kernels are applied, beam hardening reduced reconstructions with maintained image impression can be achieved (Fig. 6d).

V. CONCLUSION

In this paper, an image-based beam hardening reduction algorithm that combines material density distribution with a polychromatic model of X-ray propagation is introduced. The algorithm has been implemented for a 3D cone beam geometry and was shown to yield excellent results in reducing cupping and streak artifacts. During iterations, segmentations with density information is retained to achieve more accurate results for reproducing a polychromatic model in forward projecting. In contrast to other iterative BHC approaches, our method distinctly preserves better original reconstruction information, which facilitates faster convergence. A spatial resolution matching technique is applied in order to improve image quality and overall performance.

Disclaimer: The concepts and information presented in this paper are based on research and are not commercially available.

REFERENCES

- [1] M. Kachelrieß, K. Sourbelle, and W. A. Kalender, "Empirical cupping correction: a first-order raw data pre-correction for cone-beam computed tomography." *Med Phys*, vol. 33, no. 5, pp. 1269–1274, May 2006.
- [2] R. E. Alvarez and A. Macovski, "Energy-selective reconstructions in x-ray computerised tomography," *Physics in Medicine and Biology*, vol. 21, no. 5, p. 733, 1976.
- [3] J. P. Stonestrom, R. E. Alvarez, and A. Macovski, "A framework for spectral artifact corrections in x-ray CT," *Biomedical Engineering, IEEE Transactions on*, vol. BME-28, no. 2, pp. 128–141, Feb. 1981.
- [4] P. Stenner, T. Berkus, and M. Kachelrieß, "Empirical dual energy calibration (EDEC) for cone-beam computed tomography," *Medical Physics*, vol. 34, no. 9, pp. 3630–3641, 2007.
- [5] C. Maaß, E. Meyer, and M. Kachelrieß, "Exact dual energy material decomposition from inconsistent rays (MDIR)," *Medical Physics*, vol. 38, no. 2, pp. 691–700, 2011.
- [6] G. Herman, "Correction for beam hardening in computed tomography," *Physics in Medicine and Biology*, vol. 24, p. 81, 1979.
- [7] E. V. de Castele, "Model-based approach for beam hardening correction and resolution measurements in microtomography," Ph.D. dissertation, University Antwerpen, 2004.
- [8] J. Hsieh, R. C. Molthen, C. A. Dawson, and R. H. Johnson, "An iterative approach to the beam hardening correction in cone beam CT," *Medical Physics*, vol. 27, no. 1, pp. 23–29, 2000.
- [9] B. de Man, J. Nuyts, P. Dupont, G. Marchal, and P. Suetens, "An iterative maximum-likelihood polychromatic algorithm for CT," *IEEE Trans. Med. Imaging*, vol. 20, no. 10, pp. 999–1008, 2001.
- [10] I. Elbakri and J. Fessler, "Segmentation-free statistical image reconstruction for polyenergetic x-ray computed tomography with experimental validation," *Physics in Medicine and Biology*, vol. 48, p. 2453, 2003.
- [11] M. Kachelrieß and W. Kalender, "Improving PET/CT attenuation correction with iterative ct beam hardening correction," in *Nuclear Science Symposium Conference Record (NSS/MIC)*, vol. 4, 2005.
- [12] H. Gao, L. Zhang, Z. Chen, Y. Xing, and S. Li, "Beam hardening correction for middle-energy industrial computerized tomography," *IEEE Transactions on Nuclear Science*, vol. 53, no. 5, p. 2796, 2006.
- [13] M. Krumm, S. Kasperl, and M. Franz, "Reducing non-linear artifacts of multi-material objects in industrial 3d computed tomography," *NDT & E International*, vol. Vol 41, No 4, pp. 242–251, 2008.
- [14] G. V. Gompel, K. V. Slambrouck, M. Defrise, K. J. Batenburg, J. de Mey, J. Sijbers, and J. Nuyts, "Iterative correction of beam hardening artifacts in CT," *Medical Physics*, vol. 38, no. S1, pp. S36–S49, 2011.
- [15] "NIST, the national institute of standards and technology." <http://physics.nist.gov/physrefdata/xraymasscoef/cover.html>, 2011.
- [16] W. H. Press, S. A. Teukolsky, W. T. Vetterling, and B. P. Flannery, *Numerical Recipes – The Art of Scientific Computing*, 3rd ed. Cambridge University Press, 2007.
- [17] M. Tian, Q. Yang, A. Maier, I. Schasiepen, N. Maass, and M. Elter, "An automatic histogram-based initializing algorithm for K-means clustering in CT," in *Proceedings des Workshops Bildverarbeitung für die Medizin 2013*, 2013, pp. 277–282.
- [18] <http://www.imp.uni-erlangen.de/phantoms/hip/hipphantom.html>.
- [19] L. A. Feldkamp, L. C. Davis, and J. W. Kress, "Practical cone-beam algorithm," *Journal of the Optical Society of America*, vol. 1, pp. 612–619, 1984.